JOURNAL OF SPACECRAFT AND ROCKETS
Vol. 42, No. 3, May–June 2005

Transpiration Cooling Performance in LOX/Methane Liquid-Fuel Rocket Engines

Andrea Bucchi* and Claudio Bruno†
University of Rome "La Sapienza," 00184 Rome, Italy
and
Alessandro Congiunti‡
Avio S.p.a., Colleferro, 00034 Rome, Italy

A transpiration cooling model that uses high-pressure real gas properties has been developed to determine transpiration cooling performance of methane in the throat region of a high-thrust, high-pressure LOX/LCH_4 liquid-fuel rocket engine, such as those currently being investigated in the European Union. The model is a series of nonlinear one-dimensional ordinary differential equations for the conduction–convection of heat between the coolant and the porous material and neglects vapor formation for simplicity. This last assumption occurs, in fact, only with low thermal conductivity materials (k_{wall} = 20 W/mK) and at low coolant-injection temperature (T_{cool_in} = 140 K), these conditions being present in only 3 of the 21 cases examined in the parametric analysis. Only steady-state results are presented; comparisons to test data were not made, because experiments to this purpose are still in the planning process. Temperature profiles along the liner wall have been numerically obtained by varying liner porosity (ε = 15–17%), conductivity (k_{wall} = 20 and 100 W/mK), and coolant injection temperature (T_{cool_in} = 140 and 300 K). Results indicate that profiles of temperature, pressure, and density tend to have sharp gradients near the hot gas–porous wall interface. They also show that very low surface temperatures (T_{max} = 500, 600, and 700 K) are possible with a methane transpiration flowrate corresponding to about 5%, or less, of that injected into the combustion chamber. The associated specific impulse loss due to the flowrate of injected coolant may be at least partially recovered by the increase of turbopump efficiency, because pressure losses in the cooling circuit are substantially reduced; furthermore, based on predicted wall temperature, reusability appears potentially higher than that obtainable with other regenerative cooling systems.

Nomenclature

A	=	area, m^2
a, b	=	coefficients
B_0	=	permeability, m^2
BR	=	blowing ratio
C_p	=	specific heat at constant pressure, J/kgK
CR	=	coolant ratio
c^*	=	characteristic velocity, m/s
D_t	=	throat diameter, m
Dq	=	heat flux error, W/m^2
Dp	=	pressure error (matching condition), Pa (bar)
d	=	characteristic dimension (in Re), m
$f(x)$	=	generic function
G	=	generic quantity (error definition)
G_{cool}	=	coolant mass-flow rate (per unit area), kg/m^2s
h	=	heat transfer coefficient, W/m^2K
h_v	=	volumetric heat transfer coefficient, W/m^3K
I_{sp}	=	specific impulse, s
K_M	=	molecular weight ratio
K_T	=	temperature ratio
k	=	thermal conductivity, W/mK
M	=	Mach number
$\dot{m}$	=	coolant mass flow rate, kg/s
N	=	total number of nodes
Nu	=	Nusselt number
P	=	pressure, Pa (bar)
Pr	=	Prandtl number
q	=	heat flux, W/m^2
R_t	=	throat radius, m
r	=	recovery factor
r_{curv}	=	nozzle curvature radius, m
r_p	=	radius of "spheres" simulating porosity, m
Re	=	Reynolds number
St	=	Stanton number with blowing
St_0	=	Stanton number without blowing
T	=	temperature, K
t	=	wall thickness, m
u	=	velocity, m/s
x	=	coordinate from coolant side to hot gas side of material, m
γ	=	heat specific ratio
ε	=	porosity
μ	=	dynamic viscosity, $Pa \cdot s$
ρ	=	density, kg/m^3
σ	=	defined in Bartz formula
Φ	=	equivalence ratio
ω	=	exponent of the viscosity-temperature relation

Subscripts

ad.wall	=	adiabatic wall (temperature)
Bartz	=	Bartz formula
CH_4	=	methane
comb	=	combustion chamber
cool, coolant	=	coolant
cool_in	=	coolant at inlet
cool_out	=	coolant at wall exit
cr	=	critical conditions
fuel_in	=	fuel inlet properties

Received 14 January 2004; revision received 14 March 2004; accepted for publication 10 May 2004.

*Aerospace Engineer, Department of Mechanics and Aeronautics; bucchi.andrea@libero.it.
†Associate Professor, Department of Mechanics and Aeronautics; c.bruno@dma.ing.uniromal.it. Associate Fellow AIAA.
‡Aerospace Engineer, Space Propulsion Design Department; alessandro.congiunti@aviogroup.com.

gas	=	bulk hot gas
LOX	=	liquid oxygen
max	=	maximum value
ox_in	=	oxidant inlet properties
porous	=	porous material
st	=	stoichiometric
surface	=	surface hot gas side
wall	=	wall material properties
0	=	stagnation properties

Superscript

$*$	=	shielding effect (heat flux)

Introduction

REQUIREMENTS for the next liquid-fuel rocket engine (LRE) generation include lower costs (production, insurance, maintenance, and operational), more reliability (0.01% failure probability per mission: the same risk as that of losing a military jet fighter), more durability, and better performance (for example, higher thrust-to-weight ratio).

Lower costs may be achieved with a long-life design. Essentially, this means keeping the temperature under control to minimize the high thermal and mechanical stresses typical of LRE structures.

Looking at conventional regenerative-cooling strategies, new concepts in cooling systems are required. A classic example, the space shuttle main engine, uses a classic regenerative-cooling system; liquid hydrogen flows at high speed in the coolant channels to control heat transfer and cool the engine walls before injection. This solution involves high pressure drops and power required by the turbopump feed system, resulting in high system weight.

A second problem typical of regenerative cooling is known as thermal ratcheting[1]: thermal cycling drives large plastic strain in the wall separating coolant from hot gas. With time, the wall becomes thinner, with a high probability of developing cracks.

Among recent concepts to improve cooling are[2] improved liner material (ICL), elastic liner (EL), microchannel cooling structure (MCS), thermal barrier coating (TBC), and transpiration cooling.

Some of these solutions control the damaging effects of high heat transfer by using materials with higher conductivity and greater ultimate strength (ICL), or by deliberately allowing the structure to elastically deform (EL).

The MCS solution reduces the pressure drop in the regenerative cooling system by means of high-aspect-ratio coolant channels, requiring lower coolant speed, but it is also expensive.

Future reusable LRE systems need life enhancement by a factor of 10, and most of these approaches cannot realize it. The critical issue is, in fact, the reduction in the ultimate stress of most metallic materials with increasing temperature.

Transpiration cooling[3] (active technique) and TBC (passive technique) address this issue by limiting the effective heat flux acting on the structures. It therefore seems natural to investigate transpiration cooling as a way to improve engine life, because this system allows, in principle, very low wall temperature (500–700 K).

Many mathematical models have been developed in the past to describe coolant flow into a porous material. The governing equations in these models require global parameters (such as porosity, permeability, and thermal conductivity) to describe porous-material behavior. A critical step in modeling transpiration cooling for propulsive applications (e.g., nozzle cooling) is to estimate the effective heat transfer between the hot gas and the porous wall where mixing between combustion gas and injected coolant takes place.

The goal of this work is to provide an assessment of the transpiration cooling performance of LCH_4 in future large LRE using LOX and LCH_4 as propellants. Such a combination is, in fact, the object of much interest in the European Union (EU) at this time.[4]

An additional incentive for studying transpiration cooling is the issue of reusability, suggesting that engine wall temperatures be kept as low as economically possible. Avoiding direct contact between hot products and walls by using transpiration appears, in this context, a good potential strategy.

Because the EU has no prior experience in transpiration cooling, such an assessment should provide basic understanding, which it is hoped will quickly point out the pluses and minuses of this technology. Because of time constraints, the model presented here is topological for simplicity, although independently developed supercritical fluid properties[4] have been utilized to better characterize the coolant (LCH_4).

An efficiency parameter, the coolant ratio (CR), has been introduced to estimate the total fuel mass flow requirement (used as coolant) compared to that burned in the combustion chamber; CR helps in evaluating the cost advantage (or disadvantage) of a transpiration cooling system capable, in principle, of enhancing engine life.

It is chiefly progress in material technology (especially composite materials) that enables the development of transpiration cooling. The first attempt in a LRE was in the 1960s when John Chamberlain (at Pratt and Whitney)[5] designed the engine for the future space shuttle. The combustion chamber and nozzle throat were formed from many copper wafers stacked together; this system did not use any porous material, but a form of transpiration cooling was obtained just the same by small involute coolant passages etched into each copper wafer. The most important feature of this design (separate wafers) is shown in this work to be a powerful solution to optimizing the transpiration cooling system and at the same time avoiding axial thermal gradients and transverse (oblique) coolant flow.

Transpiration Cooling

In transpiration cooling (Fig. 1), the coolant (typically fuel: liquid hydrogen or, as in this study, methane) is injected through a porous material. In this paper we examine the effect of this cooling technique on a porous material constituting the nozzle throat region.

The primary heat exchange takes place between the coolant flow and the porous material: the coolant gets warmer (via conduction–convection heat transfer) and the porous material cooler. A second heat exchange takes place through the thickened boundary layer on the gas side produced by coolant injection, with the coolant film reducing the heat transfer between the porous wall and the hot gas.

The critical zone in a rocket engine is the nozzle throat region; in fact, the maximum heat transfer (up to 160 MW/m^2) (Ref. 6) is reached there because the boundary layer has minimum thickness.[7]

Mathematical Model

To enhance engine life the cooling system must limit wall temperature. Because heat transfer is influenced by material porosity

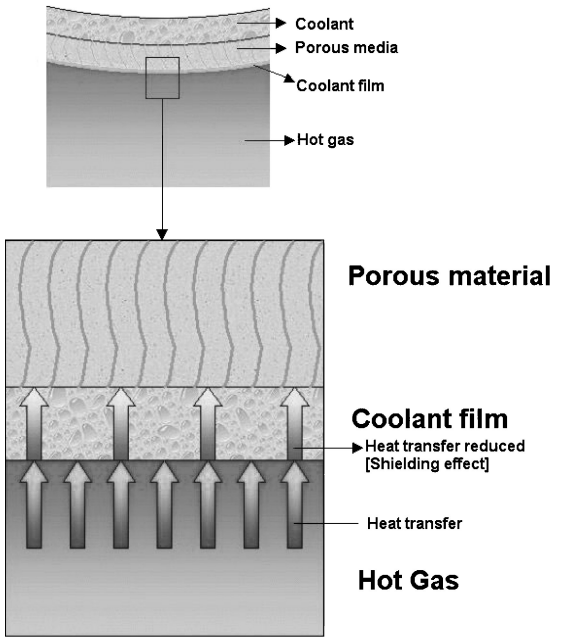

Fig. 1 Transpiration cooling.

and coolant temperature, we must predict the temperature profile through the porous material and what factors influence it most.

The coolant emerging from the pores is injected into the hot-gas stream, so that one of the physical constraints in modeling transpiration is that the coolant pressure at the pore exit equals the hot-gas pressure. Hence, the coolant pressure profile must also be predicted.

The mathematical model that follows is the simplest possible (one-dimensional) and includes three ordinary differential equations predicting porous material temperature $T_{\text{porous}}(x)$, coolant temperature $T_{\text{cool}}(x)$, and coolant pressure $P_{\text{cool}}(x)$ (see the Nomenclature).

The model equations are as follows.

Energy equation in the porous material:

$$k_{\text{porous}} \frac{\mathrm{d}^2 T_{\text{porous}}}{\mathrm{d}x^2} = h_v [T_{\text{porous}} - T_{\text{cool}}] \tag{1}$$

The left-hand side (LHS) of Eq. (1) is the conduction into the porous material; the right-hand side (RHS) describes synthetically the heat transfer between the porous material and the coolant. The variable x is the coordinate along the nozzle radius.

This second-order ordinary differential equation needs two boundary conditions (BC):

$$T_{\text{porous}}(x = 0) \rightarrow \text{assigned} \tag{1a}$$

The wall temperature in contact with coolant is assumed to be known or imposed, with $x = 0$ determining where the wall is in contact with the liquid coolant. The second BC requires the heat transfer into the porous material (conduction heat transfer) to be equal to that from the hot gas, accounting for the shielding effect of transpiration:

$$q^* = -k_{\text{porous}} \left. \frac{\mathrm{d}T_{\text{porous}}}{\mathrm{d}x} \right|_{x=t} \tag{1b}$$

where $x = t$ is the location of the wall–hot-gas interface.

Coolant energy equation:

$$\frac{\mathrm{d}T_{\text{cool}}}{\mathrm{d}x} = \frac{h_v}{G_{\text{cool}} C p_{\text{cool}}} (T_{\text{porous}} - T_{\text{cool}}) \tag{2}$$

The RHS of (2) describes synthetically the heat transfer between the porous material and the coolant. Its BC is

$$T_{\text{cool}}(x = 0) \rightarrow \text{assigned} \tag{2a}$$

because the coolant injection temperature is assumed to be known.

Coolant pressure equation (Darcy law):

$$\frac{\mathrm{d}P_{\text{cool}}}{\mathrm{d}x} = -\frac{\mu_{\text{cool}} G_{\text{cool}}}{\rho_{\text{cool}} B_0} \tag{3}$$

This ordinary differential equation needs only one BC,

$$P_{\text{cool}}(x = 0) \rightarrow \text{assigned} \tag{3a}$$

because the coolant-injection pressure is typically imposed or known.

Modeling Transport Terms in the Mathematical Model

As a first approximation, the thermal conductivity in the porous material (k_{porous}) can be related to the material properties through the porosity ε (a sort of scaling factor):

$$k_{\text{porous}} = k_{\text{wall}} (1 - \varepsilon) \tag{4}$$

where ε is the void fraction in the porous material constituting the nozzle wall.

The volumetric heat-transfer coefficient h_v is modeled as

$$h_v(T) = Nu k_{\text{cool}} / B_0 \tag{5}$$

Nu is the Nusselt number, estimated in a porous material by Florio's formula,[8]

$$Nu = a Re^b \tag{5a}$$

where $a = 2.22 \times 10^{-6}$, $b = 0.703$. For a porous material the Reynolds number ($Re = \rho u d / \mu$) with use of the Darcy law [see Eq. (3)] is defined as[8,9]

$$Re = \frac{\rho_{\text{cool}}}{\mu_{\text{cool}}} \left(-\frac{B_0}{\mu_{\text{cool}}} \frac{\mathrm{d}P}{\mathrm{d}x} \right) d = -\frac{\rho_{\text{cool}} B_0^{1.5}}{\mu_{\text{cool}}^2 \varepsilon} \frac{\mathrm{d}P}{\mathrm{d}x} \tag{5b}$$

where d is defined as

$$d = \sqrt{B_0} / \varepsilon \tag{5c}$$

Other formulas suggested for d are in the literature.[9]

The permeability coefficient B_0 of the porous material is modeled (crudely) as that of a packed bed of spheres of radius r_P, so that B_0 can be evaluated by the Brennan–Kroliczek relationship between porosity and permeability[10]:

$$B_0 = \frac{\left(2 r_p^2\right) \varepsilon^3}{150 (1 - \varepsilon)^2} \tag{6}$$

To evaluate the heat flux q from the gas in high-speed flows, and therefore q^*, needed in Eq. (1b), it is convenient to introduce the adiabatic wall temperature $T_{\text{ad.wall}}$ associated with the turbulent-boundary-layer heating due to viscosity:

$$T_{\text{ad.wall}} = T_{\text{gas}} + r (T_{0\text{gas}} - T_{\text{gas}}) \tag{7a}$$

where $r = \sqrt{(Pr)}$ for laminar flow, $r = \sqrt[3]{(Pr)}$ for turbulent flow, and $T_{0\text{gas}}$ is the total gas temperature. For an ideal gas (at high temperature the real gas behavior is similar to the ideal gas behavior)

$$T_{0\text{gas}} = \{1 + [(\gamma - 1)/2] M^2\} T_{\text{gas}} \tag{7b}$$

and with the Bartz formula for q (valid only in the region near the nozzle throat)

$$q = q_{\text{Bartz}} = h_{\text{Bartz}} (T_{\text{ad.wall}} - T_{\text{surface}}) \tag{7c}$$

or

$$q_{\text{Bartz}} = h_{\text{Bartz}} \left(\left\{ 1 + \sqrt[3]{Pr} [(\gamma - 1)/2] M^2 \right\} T_{\text{gas}} - T_{\text{surface}} \right) \tag{7d}$$

with T_{surface} the surface temperature of the porous material on the hot-gas side.

The heat-transfer coefficient with the Bartz formula[7,11] is

$$h_{\text{Bartz}} = \left\{ \left[0.026 \Big/ (D_t)^{0.2} \right] \left(\mu^{0.2} c_P \Big/ Pr^{0.6} \right)_0 \times \left(P_0 \Big/ c^* \right)^{0.8} (D_t / r_{\text{curv}})^{0.1} \right\} (A^*/A)^{0.9} \sigma \tag{8}$$

where D_t is the throat nozzle diameter; r_{curv} is the local radius of curvature; $A^*$is the throat area; and A is the area of a generic nozzle section. In Eq. (8) $c^* = P_0 A^* / \dot{m}$ is the characteristic velocity and σ is defined as

$$\sigma = 1 \Big/ \left(\tfrac{1}{2} (T_{\text{surface}} / T_{0\text{gas}}) \{1 + [(\gamma - 1)/2] M^2\} + \tfrac{1}{2} \right)^{0.8 - 0.2\omega} \times \{1 + [(\gamma - 1)/2] M^2\}^{0.2\omega} \tag{8a}$$

$\gamma = c_P / c_V$ the specific heat ratio of combustion gases. ω is the exponent of the viscosity–temperature relation $\mu \propto T^{\omega}$ ($\omega \cong 0.67$ for diatomic gases). The shielding effect due to transpiration (and q^*) can be evaluated by using the Stanton number. This effect scales with the "blowing" Stanton number,[12]

$$St = \frac{\text{heat transfer in } \perp \text{ flow direction}}{\text{heat transfer in } // \text{ flow direction}} = \frac{h}{\rho u C p} = \frac{Nu}{Re \cdot Pr} \tag{9a}$$

The Stanton number St_0 without blowing is

$$St_0 = h_{\text{Bartz}}/\rho_{\text{gas}}u_{\text{gas}}Cp_{\text{gas}} \tag{9b}$$

The shielding effect due to the boundary layer, from a simplified one-dimensional thermal-energy balance, can be calculated from[12]

$$\frac{St}{St_0} = \frac{(\text{BR}/St_0)K_M K_T}{e^{(\text{BR}/St_0)K_M K_T} - 1} \tag{9c}$$

where

$$K_M = \left[\frac{(\text{molecular weight})_{\text{gas}}}{(\text{molecular weight})_{\text{coolant}}}\right]^{0.6} \tag{9d}$$

$$K_T = \left(\frac{T_{\text{ad.wall}}}{T_{\text{surface}}}\right)^{0.2\ldots0.4} \tag{9e}$$

and where BR is the blowing ratio, to be defined.

In conclusion, not the whole heat flux q_{Bartz} reaches the wall, but only part of it, q^*_{Bartz} [as in Eq. (1b)]:

$$h^*_{\text{Bartz}} = h_{\text{Bartz}}\frac{St}{St_0} = \frac{h_{\text{Bartz}}}{St_0}\left[\frac{\text{BR}\cdot K_M\cdot K_T}{e^{(\text{BR}/St_0)K_M K_T} - 1}\right] \tag{9f}$$

$$q^*_{\text{Bartz}} = h^*_{\text{Bartz}}(T_{\text{ad.wall}} - T_{\text{surface}}) = q^* \tag{9g}$$

Blowing Ratio

The critically important coefficient BR is the ratio between the injected coolant mass flow rate and hot gas mass flow rate:

$$\text{BR} = \frac{\rho_{\text{cool}}u_{\text{cool}}}{\rho_{\text{gas}}u_{\text{gas}}} = \frac{G_{\text{cool}}}{\rho_{\text{gas}}u_{\text{gas}}} \tag{10}$$

The heat transfer between porous material and hot gas is controlled by the boundary-layer thickness. A high BR produces thicker boundary layers and a large decrease in heat transfer between the wall and the hot gas; see Eq. (9f). However, it also reduces the effective nozzle throat area, an effect to be dealt with during the LRE design phase. A second critical aspect associated with BR is that the coolant injected through the porous material in the nozzle is not used for propulsion, lowering I_{sp}. This negative effect is gauged by the coolant ratio CR (Ref. 3):

$$\text{CR} = (\dot{m}_{\text{fuel}})_{\text{transpiration}}/(\dot{m}_{\text{fuel}})_{\text{combustion}} = \dot{m}_{\text{cool}}/\dot{m}_{\text{fuel}} \tag{11}$$

CR can be viewed as an efficiency parameter in transpiration cooling. A lower CR indicates a better cooling system (higher efficiency), because less fuel is diverted and injected into the nozzle and so more can burn inside the combustion chamber.

Computational Solution

Equations (1–3) were solved iteratively until they converged by a novel code with use of an explicit finite-difference method and by dividing the computational $0 \le x \le t$ domain into N nodes.

The number of nodes N was varied from 100 to 1000 to test grid independence. Using $N = 1000$ produced acceptable convergence with a reasonable CPU time (2 h); see the Appendix for details.

The transpiration cooling system has been assumed (and analyzed) to be astride the nozzle throat, its overall length being $2R_t$ (Figs. 2 and 3).

The $2R_t$ length of this region has been divided into S individual sections or slices.

The heat-transfer problem has been analyzed as a one-dimensional radial problem in every slice. The limit of this approach is that the heat exchange for a generic S section is not influenced by heat exchange in the other sections; that is, the heat flux in the axial direction is neglected. However, as results will show, this approximation may be reasonable and is also very convenient in a preliminary performance assessment or design. In fact, to start designing

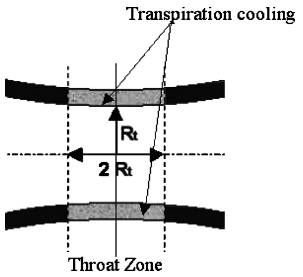

Fig. 2 Throat zone.

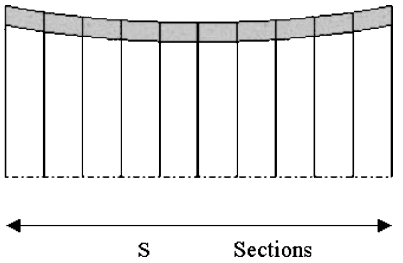

Fig. 3 Throat-zone partition.

transpiration cooling, optimization section by section seems practical, resulting in a rough but quick coolant requirements assessment in a region (throat) where the thermodynamic properties of the hot gas (especially pressure) change rapidly.

In the present calculations every slice has been assumed to be 10 mm wide, this dimension having been found convenient (like $N = 1000$) to speed up the numerical computation while maintaining accuracy (see the Appendix).

Thermodynamic properties of the nozzle gas (pressure, temperature, density, viscosity, thermal conductivity, specific heats, and their ratio) are considered radially uniform in all slices. Due to the high (supercritical) pressures typical of future liquid oxygen/hydrocarbon (LOX/HC) LRE, density and specific heats were calculated with the Lee–Kesler equation of state for real gases[4]; viscosity and thermal conductivity were evaluated with the Chung method,[4] with use of the ANACYC software developed in collaboration with Avio.[13] ANACYC provides preliminary LRE-nozzle sizing by using (quasi-one-dimensional) adiabatic flow section by section and real gas (sub- and supercritical) properties. ANACYC is also integrated with CHEMKIN v. 3.0™ to evaluate the equilibrium gas composition. Therefore engine geometry and gas thermodynamic properties (composition, pressure, temperature, density, viscosity, thermal conductivity, specific heats, and their ratio) are calculated for all S sections.

Therefore, the input to the transpiration cooling code developed in the present work is the ANACYC output, plus 1) maximum wall temperature allowed $T_{\max}$, 2) thermal conductivity of the wall material (without the effect of porosity) k_{wall}, 3) radius r_p of spheres ideally composing the material according to its permeability model (typically, $r_p = 0.01$ mm); and 4) porosity law variation (porosity was changed in 0.5% steps).

The boundary conditions at every section S were coolant injection temperature $T_{\text{cool\_in}}$, coolant injection pressure $P_{\text{cool\_in}}$, and temperature of wall in contact with coolant T_{wall}.

The transpiration cooling code produces as output 1) porous temperature $T_{\text{porous}}(x)$; 2) coolant temperature $T_{\text{cool}}(x)$; 3) coolant pressure $P_{\text{cool}}(x)$; 4) hot gas side wall temperature T_{surface}; 5) coolant "out" properties (temperature, pressure, speed, stay time, density, viscosity, thermal conductivity, specific heats); 6) wall thickness; 7) heat flux (with and without shielding effect), using the Bartz formula; 8) total coolant mass used in transpiration; 9) blowing ratio BR (local and total); and 10) coolant ratio CR (local and total).

In every section the transpiration cooling code evaluates the wall thickness and consequently the coolant mass flow rate necessary to achieve wall temperature in the allowed range; see Eq. (12).

The solution found must meet preliminary optimization criteria such as the following:

1) Low coolant ratio CR.

2) Low coolant maximum temperature: The methane coolant is subjected to coking (cracking). Carbon deposits might obstruct pores, altering the heat exchange. Recent studies[14] demonstrate no coking problem for pure methane, so long as its temperature stays below 750 K.

3) Low maximum wall temperature: This is the critical requirement for any cooling system (lower temperatures enhance engine life and pave the way toward reusability). However, too low a wall temperature is a poor solution in terms of I_{sp}, because it implies high coolant flow rates. Temperatures were imposed in the range

$$[T_{max} - 1\%] \leq T_{wall\_allowed} \leq T_{max} \tag{12}$$

This constraint obtain very low thermal gradients in the axial direction, so that neglecting axial heat transfer in the model may be considered a reasonable approximation.

Methane Phase Change

The mathematical model of Eqs. (1–3) predicts porous material temperature $T_{porous}(x)$, coolant temperature $T_{cool}(x)$, and coolant pressure $P_{cool}(x)$ at every nozzle slice; an example of the numerical solution is provided by Figs. 4–7, which show the temperature profile of the porous material and the temperature, pressure, and density profiles of the coolant. They are obtained with the following data input: slice number 27 (last nozzle section); coolant injection temperature $T_{cool\_in} = 140$ K; coolant injection pressure $P_{cool\_in} = 200$ bar; thermal conductivity $k_{wall} = 20$ W/mK; maximum wall temperature allowed $T_{max} = 500$ K; slice porosity $\varepsilon = 13\%$.

Note that at temperature $T_{cool\_in} = 140$ K and with $P_{cool\_in} = 200$ bar, methane is liquid and its density is about 402.88 kg/m^3. Along its path into the porous material methane becomes warmer and its pressure decreases. If the wall thermal conductivity is about $k_{wall} = 20$ W/mK a phase change (liquid to vapor) occurs. Consequently results presented in the parametric analysis below overestimate the coolant mass requirement, because the mathematical model (assuming supercritical conditions) does not include the latent heat of vaporization of methane. This effect is important in the last few nozzle sections (8 of 27 total sections examined), where methane must become subcritical (coolant pressure less than methane critical pressure $P_{cr} = 46.0$ bar and coolant temperature less than methane critical temperature $T_{cr} = 190.4$ K). No phase change (liquid to vapor) occurs at $k_{wall} = 100$ W/mK. Phase change of CH_4 becomes a significant problem only for very poor material conductivity.

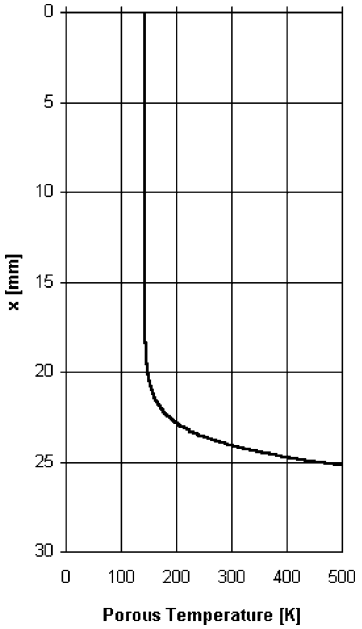

Fig. 4 Porous temperature profile.

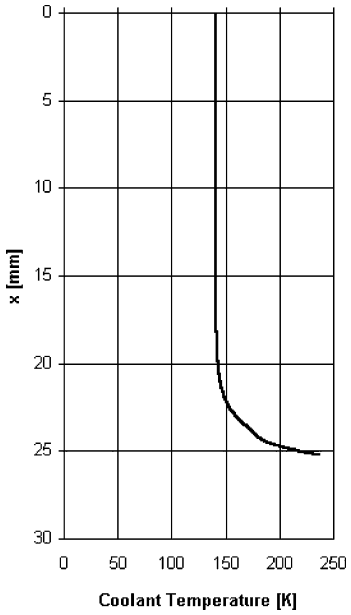

Fig. 5 Coolant temperature profile.

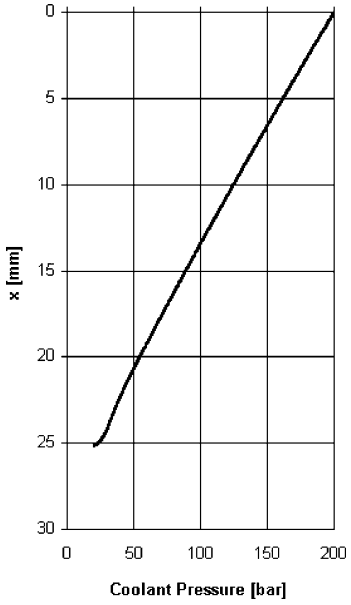

Fig. 6 Coolant pressure profile.

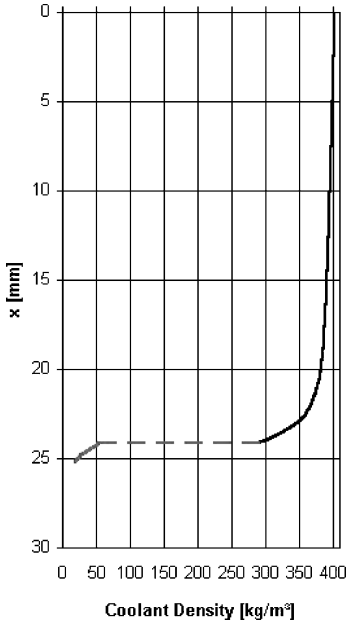

Fig. 7 Coolant density profile.

Avoiding methane phase change is a design issue because there is a sharp expansion; for example, see Fig. 7. Methane density changes from $\approx$290 kg/m^3 to vapor density $\approx$54 kg/m^3. This can cause structural failure of the porous material.

Parametric Analysis Results

The first three parameters varied were wall material thermal conductivity $k_{\text{wall}} = 20$ and 100 W/mK (relatively low); coolant injection temperature $T_{\text{cool\_in}} = 140$ K (below the methane critical temperature $T_{\text{cr}} = 190.4$ K) and 300 K (above the critical temperature); and maximum wall temperature allowed $T_{\max} = 500$, 600, and 700 K.

The fixed inputs in this particular analysis were combustion chamber pressure $P_{\text{comb}} = 200$ bar, also equal to coolant injection pressure $P_{\text{cool\_in}}$; porosity $\varepsilon = 16\%$ for the first nozzle slice/section; decreased by 0.5% every four sections along the nozzle; methane injection temperature $T_{\text{fuel\_in}} = 300$ K; oxidant (LOX) injection temperature $T_{\text{ox\_in}} = 100$ K; equivalence ratio

$$\Phi = \frac{(\dot{m}_{\text{ox}}/\dot{m}_{\text{fuel}})_{\text{st}}}{(\dot{m}_{\text{ox}}/\dot{m}_{\text{fuel}})} = \frac{3.989}{\left(\dot{m}_{\text{ox}}\big/\dot{m}_{\text{CH}_4}\right)} = 1.3$$

and thrust 2×10^6 N.

The three parameters have the following effects:

Wall Thickness

Increasing $T_{\max}$ or k_{wall} increases wall thickness t due to the lower mass flow rate of coolant required; the lower pressure drop and the pressure-matching condition together result in higher wall thickness (Figs. 8 and 9).

Coolant Speed

Coolant speed $u_{\text{cool\_out}}$ increases if $T_{\max}$ increases and the same occurs when the coolant injection temperature $T_{\text{cool\_in}}$ is raised. k_{wall} becomes important only at lower temperatures (Figs. 10 and 11).

Note that coolant velocity is low, at most 1.6 m/s; so it is its flowrate (and not its injection speed) that thickens the thermal boundary layer.

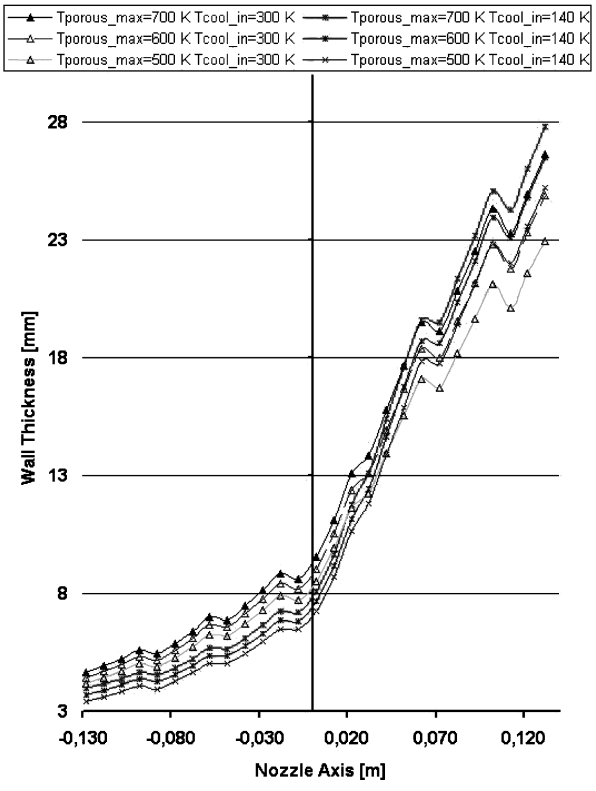

Fig. 8 Wall thickness ($k_{\text{wall}} = 20$ W/mK).

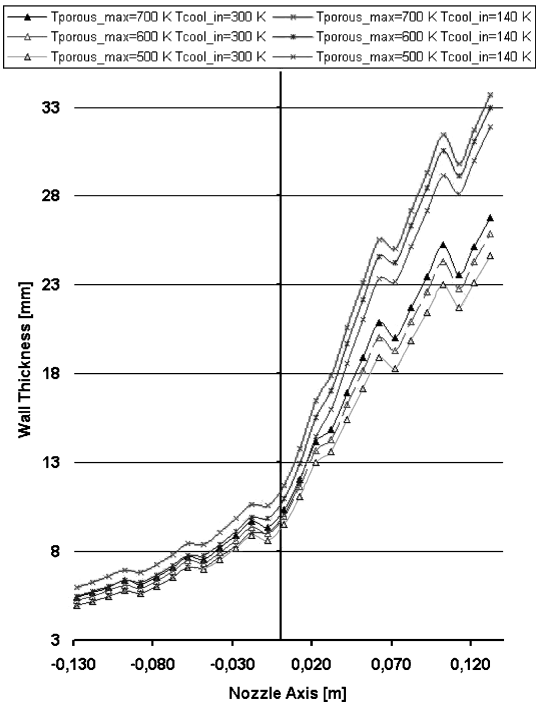

Fig. 9 Wall thickness ($k_{\text{wall}} = 100$ W/mK).

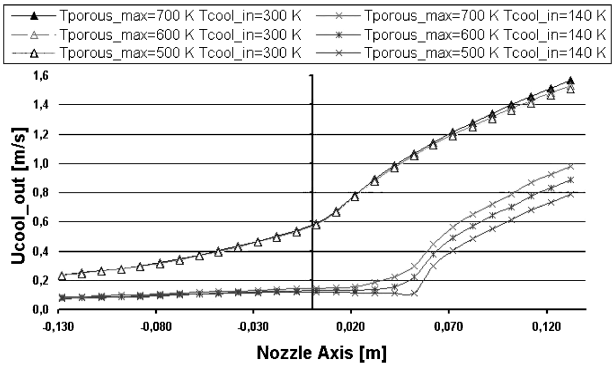

Fig. 10 Coolant velocity ($k_{\text{wall}} = 20$ W/mK).

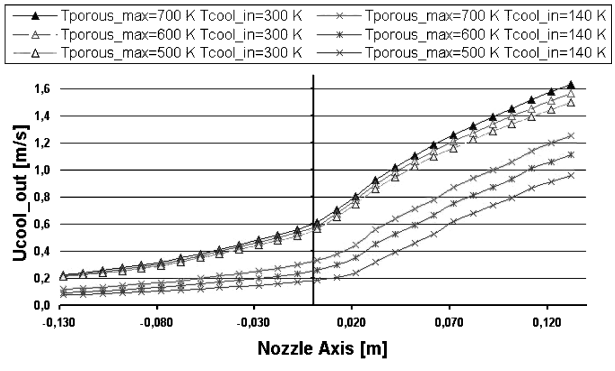

Fig. 11 Coolant velocity ($k_{\text{wall}} = 100$ W/mK).

Coolant Temperature

Coolant temperature $T_{\text{cool\_out}}$ is increased by raising $T_{\max}$ and $T_{\text{cool\_in}}$. Raising k_{wall} also raises $T_{\text{cool\_out}}$ significantly (Figs. 12 and 13).

Blowing Ratio

A higher BR shields heat more effectively; conversely, if lower $T_{\max}$ is desired BR must be increased (Figs. 14 and 15). Notice that raising $T_{\text{cool\_in}}$ from 140 to 300 K raises BR by 10%; because coolant temperature depends on engine cooling and operation this

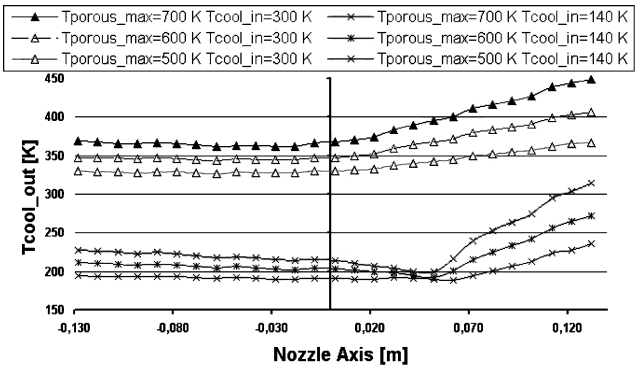

Fig. 12 Coolant temperature (k_{wall} = 20 W/mK).

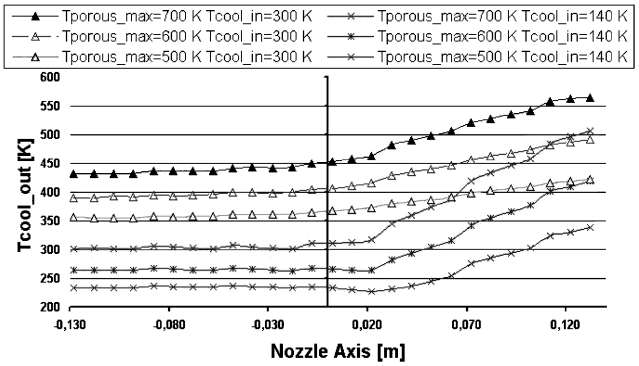

Fig. 13 Coolant temperature (k_{wall} = 100 W/mK).

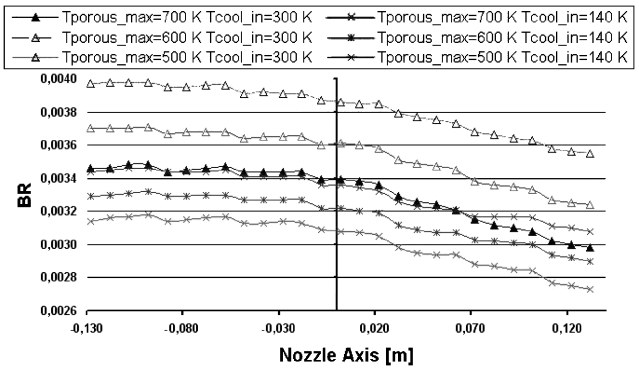

Fig. 14 Blowing ratio (k_{wall} = 20 W/mK).

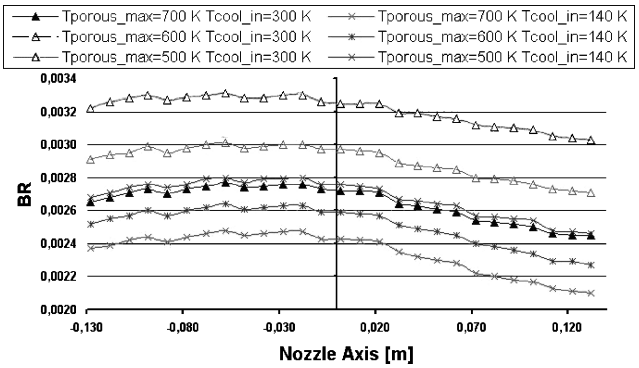

Fig. 15 Blowing ratio (k_{wall} = 100 W/mK).

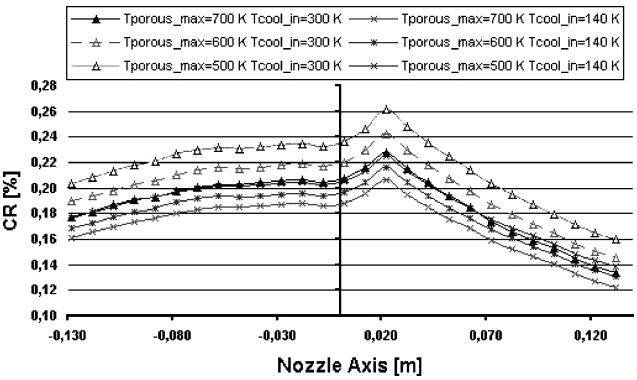

Fig. 16 Coolant ratio (k_{wall} = 20 W/mK).

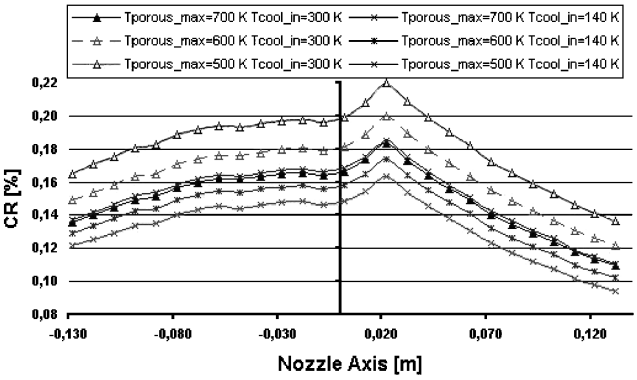

Fig. 17 Coolant ratio (k_{wall} = 100 W/mK).

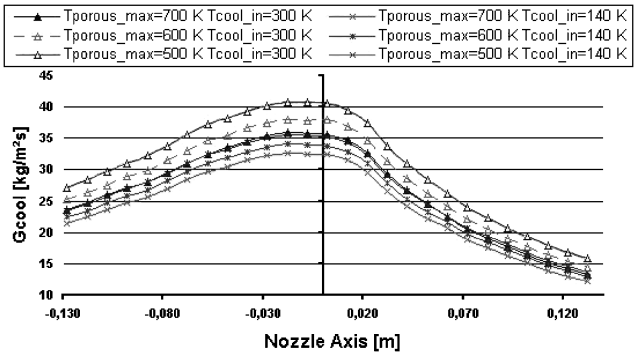

Fig. 18 Coolant mass flow rate (k_{wall} = 20 W/mK).

means that effective cooling of the throat region is possible relatively independent of overall engine configuration. Raising thermal conductivity tends to reduce BR by as much as 20%.

Coolant Ratio

Just as BR does, CR increases by 10% if T_{cool_in} is raised or T_{max} is lowered (Figs. 16 and 17). High heat flux results in a higher coolant ratio near the nozzle throat. Likewise, larger k_{wall} significantly reduces CR (about 20%); the total CR (integrated over all S slices) is in Table 1.

Coolant Mass Flow Rate G_{cool}

G_{cool} peaks at the throat section and is influenced by the way porosity changes along the nozzle axis. Predictably, G_{cool} is larger when a warmer coolant is used or T_{max} lowered (Figs. 18 and 19).

Effect of Porosity Law

Technologically, porosity is probably the most important parameter explored in this study. A parametric analysis of the effect of porosity has been performed assuming the following: coolant injection temperature $T_{cool\_in} = 300$ K; thermal conductivity

Table 1 Total CR for the entire throat zone

k_{wall}, W/mK	T_{max}, K	T_{cool_in}, K	CR_{tot}, %
20	500	300	5.845
20	600	300	5.417
20	700	300	5.073
20	500	140	5.070
100	500	300	4.909
20	600	140	4.844
20	700	140	4.626
100	600	300	4.440
100	500	140	4.104
100	700	300	4.056
100	600	140	3.843
100	700	140	3.594

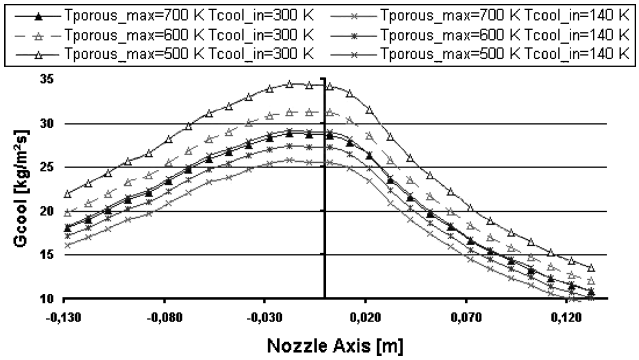

Fig. 19 Coolant mass flow rate (k_{wall} = 100 W/mK).

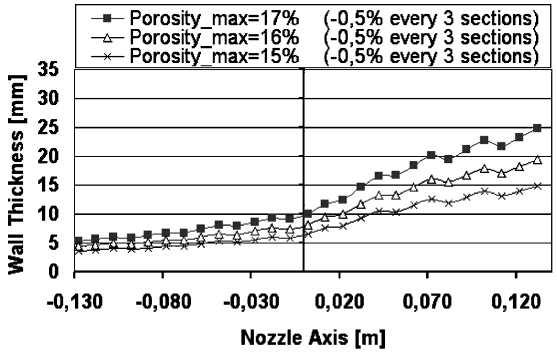

Fig. 20 Wall thickness (different porosity in the first section).

$k_{wall} = 20$ W/mK; and maximum wall temperature allowed $T_{max} = 600$ K. The remaining input data were left unchanged. The porosity ε has been changed using two different strategies:

1) Different porosities for the first nozzle section: $\varepsilon = 15\%$, 16%, and 17%. Although this is a narrow range, it is consistent with reasonable values for wall thickness. Porosity higher than 17% causes wall thickness at the last nozzle slice >31 mm, while porosity under 15% causes an extremely thin first nozzle section <3.6 mm.

2) Porosity stepped down along the nozzle axis, in three ways: decreasing by 0.5% every four sections (4 cm), or decreasing by 0.5% every three sections (3 cm), or decreasing by 0.5% every two sections (2 cm).

Porosity values in this parametric analysis are consistent with those used in a recent test at the DLR (Lampoldshausen German Aerospace Centre).[15] In this facility a carbon–carbon material with $\varepsilon \approx 20\%$ has been tested. A pyrolysis process can obtain porosity of about 15% and lower by a process allowing porosity to be varied with high reliability and precision.

Unfortunately test data of Ref. 15 could not be compared to predictions presented here, due to large differences in geometry, combustion chamber pressure, and especially coolant utilized (hydrogen).

Figures 20 and 21 show how porosity (obtained with both strategies 1 and 2) can reduce t. In fact, t varies from 7 up to 31 mm,

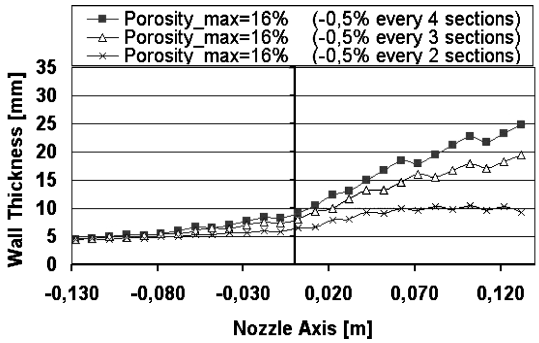

Fig. 21 Wall thickness (porosity stepped down in decrements).

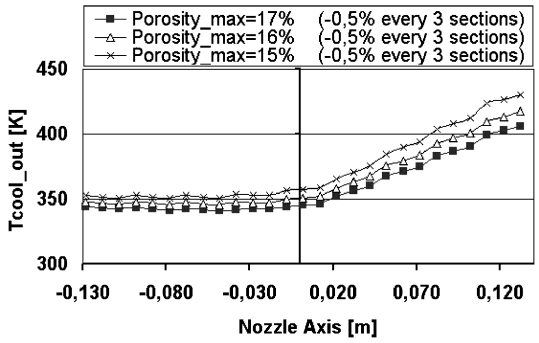

Fig. 22 Coolant temperature (different porosity in the first section).

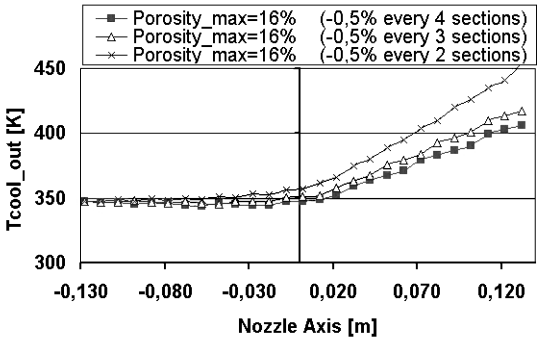

Fig. 23 Coolant temperature (porosity stepped down in decrements).

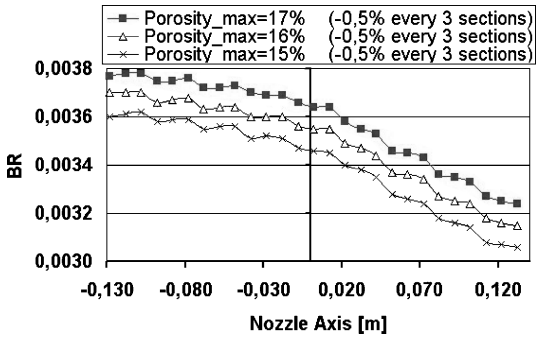

Fig. 24 Blowing ratio (different porosity in the first section).

a substantial range, due to the porosity changing along the nozzle axis. Lowering porosity lowers also material permeability and raises pressure drop so that, to meet the pressure constraint, the wall thickness must also be reduced.

Coolant velocity is weakly influenced by porosity (by no more than 1.5%) and remains very low, $\approx$ 1.6 m/s. The highest value occurs in the last section, where the maximum in the coolant-pressure gradient occurs.

Table 2 Total CR (entire throat zone)

Porosity ε (first section), %	Porosity law variation	CR_{tot}, %
17	Decrease 0.5% every 4 sections	5.547
17	Decrease 0.5% every 3 sections	5.474
16	Decrease 0.5% every 4 sections	5.417
16	Decrease 0.5% every 3 sections	5.342
17	Decrease 0.5% every 2 sections	5.323
15	Decrease 0.5% every 4 sections	5.282
15	Decrease 0.5% every 3 sections	5.204
16	Decrease 0.5% every 2 sections	5.187
15	Decrease 0.5% every 2 sections	5.034

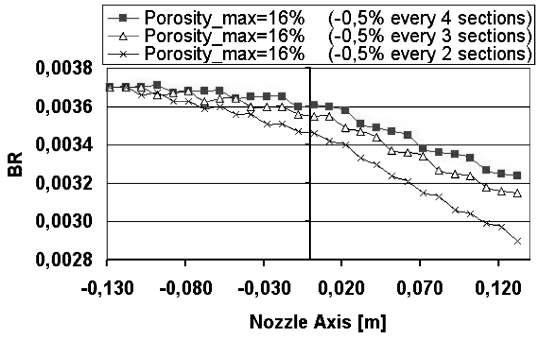

Fig. 25 Blowing ratio (porosity stepped down in decrements).

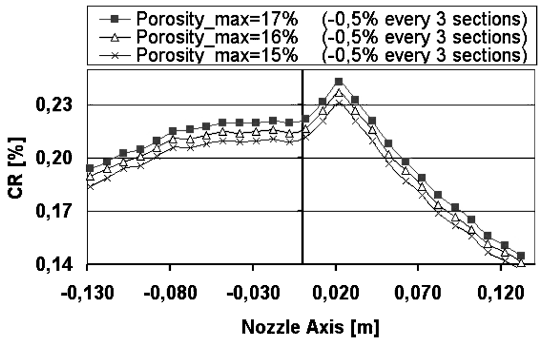

Fig. 26 Coolant ratio (different porosity in the first section).

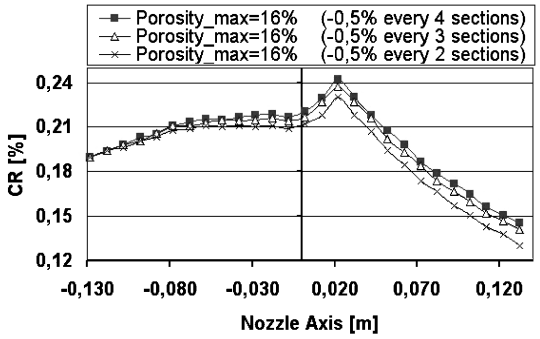

Fig. 27 Coolant ratio (porosity stepped down in decrements).

In the low range porosity increases heat transfer between the coolant and the porous material (higher volumetric heat transfer coefficient, and k_{porous} nearer to k_{wall}) so that T_{cool_out} is higher (Figs. 22 and 23).

Lower porosity also significantly lowers BR (Figs. 24 and 25), CR (see Figs. 26 and 27 and Table 2), and the coolant mass flow rate G_{cool}.

In conclusion, lowering porosity to the "right" (minimum) range has a positive effect on transpiration cooling. This is the result of competition between its effect on lowering thickness (thus less material to cool) and its effect on lowering BR (lower shielding effect on heat transfer).

Conclusions

The results of this study suggest that transpiration cooling has the potential for lowering nozzle throat wall temperature and thus enhancing engine life, with the potential payoff of reduced operation and maintenance cost.

Additionally, the regenerative cooling system feeding LCH_4 to the transpiration section will not require high-speed flow in the throat channels, implying that a lower pressure drop in the coolant circuit may reduce turbopump power.

Very low wall temperatures (500–700 K) appear within reach with moderate coolant use (less than 5%; minimum 3.6%), and even for materials with thermal conductivities well below those used in conventional cooling (e.g., four times lower than Narloy Z^{TM}).

The main factors affecting transpiration cooling are predicted to be the following:

1) Material thermal conductivity: higher k_{wall} lowers mass-flow rate, but the engine may be heavier, because wall thickness increases.

2) Porosity: an appropriate porosity drives more intense heat transfer between coolant and porous material and so lowers coolant flow rate. Porosity control is therefore a critical and enabling technology.

3) Coolant injection temperature: lower temperature achieves better heat shielding, but very low inlet temperature (e.g., $T_{cool\_in} = 140$ K) may favor vaporization of methane inside the porous material.

Transpiration cooling is not meant to replace the entire regenerative cooling system, but is rather seen as a local solution, very effective in the nozzle throat region. Using transpiration cooling to cool an entire engine would pose unacceptable coolant flow rate demands. The two cooling strategies must therefore be integrated, and with this caveat in mind design complexity can also be avoided.

Finally, some design hints are available from the parametric analysis conducted.

The partition of the nozzle throat into physically different slices is probably also a smart solution to avoid transverse (oblique) coolant flow in the axial direction and toward lower exit pressure (due to the presence of a pressure gradient along the same direction). This may be practically achieved by using a coating that inhibits porosity between two adjacent slices.

Moreover, as shown by results in this work, this solution lends itself to optimization (minimization of coolant requirement) and to better control of parameters that influence the transpiration cooling system. The main ones are

1) Porosity: uniform porosity slice by slice is required to avoid danger heat transfer peaks.

2) Wall thickness: the system is sensitive to even small thickness changes.

Appendix: Computational Time and Numerical Accuracy

Numerical solutions used a uniform grid with $N = 1000$ nodes. A higher number of nodes was found unnecessary and not advisable due to rapid growth of computational time. Computational time is governed by the following factors:

1) Total grid nodes number: Higher accuracy and computational time have opposite trends with grid nodes number N. For example, using a Pentium IV 1.8 GHz personal computer, computational times are 10–20 min for a grid with $N = 100$ nodes; 100–200 min for a grid with $N = 1000$ nodes. With the same N, CPU time differences occur for different values of the coolant injection temperature (a boundary condition).

2) Number of slices S was fixed at 27 (270 mm).

3) Computational time varies for each of the S slices. This is mostly due to the Lee–Kesler equation of state. This equation is highly accurate for real gases, but is also CPU intensive; for example, calculating density needs many iterations[4] (order of $10–10^3$)

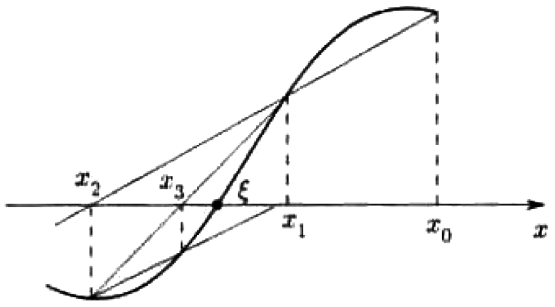

Fig. A1 Secants method with unsteady extreme points.

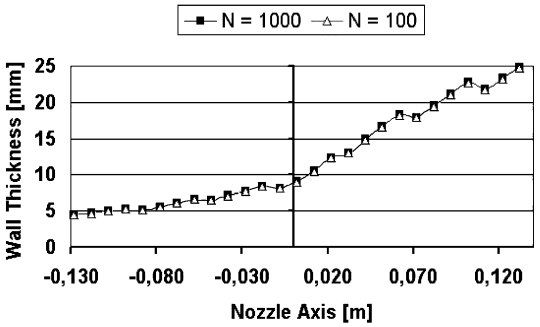

Fig. A2 Wall thickness with different grids.

depending on pressure temperature, resulting in different CPU times at different grid nodes.

4) Convergence criteria: Higher precision (lower error tolerance) affected computational time. For the porous temperature profile we accepted an error for the heat flux $|D_q| < 10$ W/m^2, compared to typical heat fluxes $\approx 10^7$ W/m^2. For pressure matching (coolant exit pressure must equal hot gas pressure) we accepted an error $|D_q| < 10$ Pa, compared to pressure $\approx 10^6$–10^7 Pa. The constraint on maximum wall temperature is Eq. (12).

5) Convergence algorithm: This algorithm is an evolution of the classical bisection method called the "secants method with unsteady extreme points." Figure A1 illustrates the method applied to a generic function $f(x)$ to find its zero at ξ in the range $[a, b]$. Iterations are calculated by the formula

$$x_{n+1} = x_n - f(x_n)\frac{x_n - x_{n-1}}{f(x_n) - f(x_{n-1})} \tag{A1}$$

where x_0, x_1 are known.

6) Grid independence: This was assessed in the following case.

Coolant injection pressure $P_{\text{cool\_in}} = 200$ bar; coolant injection temperature $T_{\text{cool\_in}} = 300$ K; wall temperature (coolant side) $T_{\text{wall}} = 300$ K; maximum wall temperature allowed $T_{\max} = 600$ K; wall material thermal conductivity $k_{\text{wall}} = 20$ W/mK; porosity for the first nozzle section $\varepsilon = 16\%$. Porosity is decreased by 0.5% every four sections along the nozzle axis. Equivalence ratio: $\Phi = 1.3$.

Nodes for the uniform grid: $N = 1000$ and 100 uniformly spaced nodes. The percent error of a generic quantity G was defined as

$$\text{error}_G = \frac{G_{[N=1000]} - G_{[N=100]}}{G_{[N=1000]}} \tag{A2}$$

This error is lower for the upstream nozzle slices, growing along the nozzle, because a radially thicker slice results in larger node spacing, lowering numerical precision. Table A1 summarizes the maximum error.

The lowest percent error occurs for wall thickness (Figs. A2 and A3), the highest for coolant ratio (Figs. A4 and A5).

Grids with low nodes number ($N = 100$) are useful only for quick estimates of the influence of a parameter; grids with high nodes number ($N = 1000$) give more reliable numerical values.

Table A1 Percent error

Output	$N = 1000$	$N = 100$	Error, %
Thickness t, mm	18.3878	18.2399	+0.80
$T_{\text{cool\_out}}$, K	406.12	397.73	+2.07
BR	0.00324	0.00331	−2.16
CR, %	0.145	0.149	−2.46
CR_{tot}, %	5.417	5.481	−1.19
G_{cool}, kg/m^{2}s	14.4349	14.7485	−2.17

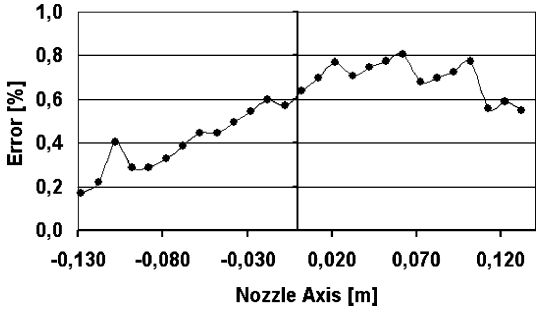

Fig. A3 Wall thickness: percent error.

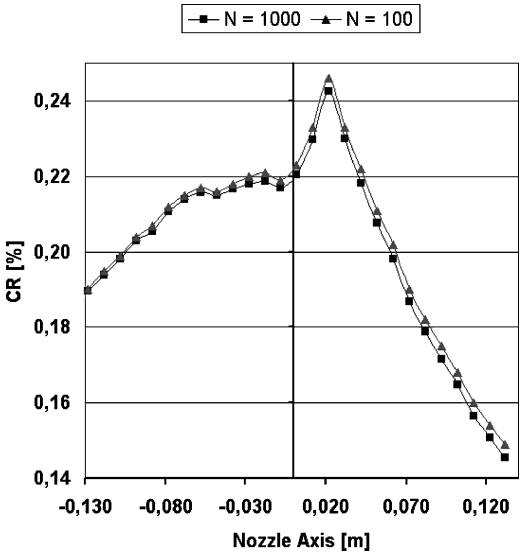

Fig. A4 Coolant ratio with different grids.

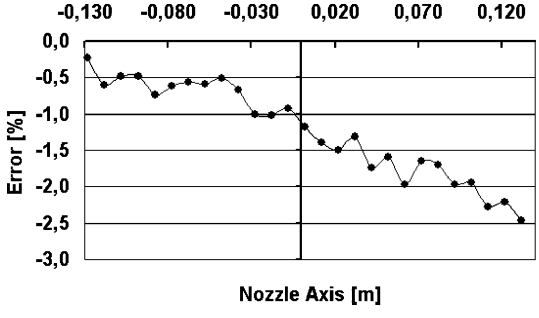

Fig. A5 Coolant ratio: percent error.

Acknowledgment

This paper is partly based on Paper IAC-03-S.3.08 presented at the 54th International Astronautical Congress, Bremen, Germany, 29 September–30 October 2003.

References

[1]Quentmeyer, R. J., "Rocket Combustion Chamber Life-Enhancing Design Concepts," AIAA Paper 90-2116, July 1990.

[2]Popp, M., and Schmidt, G., "Rocket Engine Combustion Chamber Design Concepts for Enhanced Life," AIAA Paper 96-3303, July 1996.

[3]Bucchi, A., Congiunti, A., and Bruno, C., "Investigation of Transpiration Cooling Performance in LOX/Methane Liquid Rocket Engines," 54th International Astronautical Congress, Paper IAC-03-S.3.08, Sept. 2003.

[4]Congiunti, A., Bruno, C., and Giacomazzi, E., "Supercritical Combustion Properties," AIAA Paper 2003-478, Jan. 2003.

[5]Mulready, D., *Advanced Engine Development at Pratt & Whitney (The Inside Story of Eight Special Projects, 1946–1971)*, SAE International, Warrendale, PA, 2001, pp. 87–101.

[6]Sutton, G. P., *Rocket Propulsion Elements (An Introduction to the Engineering of Rockets)*, 6th ed., Wiley, New York, 1992, pp. 89–99.

[7]Hill, P. G., and Peterson, C. R., *Mechanics and Thermodynamics of Propulsion*, 2nd ed., Addison Wesley, New York, 1992, pp. 541–551.

[8]Glass, D. E., Dilley, A. D., Kelly, H. N., "Numerical Analysis of Convection/Transpiration Cooling," NASA TM-1999-209828, Dec. 1999.

[9]Bear, J., *Dynamics of Fluids in Porous Media*, 1st ed., Dover, New York, 1988, pp. 119–135.

[10]Landis, J. A., "Numerical Study of a Transpiration Cooled Rocket Nozzle," M.S. Thesis, School of Engineering, Air Force Inst. of Technology, AFIT/GA/ENY/95D-01, Wright–Patterson AFB, OH, Dec. 1995.

[11]Landis, J. A., and Bowman, W. J., "Numerical Study of a Transpiration Cooled Rocket Nozzle," AIAA Paper 96-2580, July 1996.

[12]Serbest, E., Haidn, O. J., Meinert, J., and Huhn, J., "Investigation on the Effect of Foreign Gas Transpiration on a Turbulent Boundary Layer," AIAA Paper 2000-3386, July 2000.

[13]Congiunti, A., Ierardo, N., Cuoco, F., and Bruno, C., "High Pressure Methane Cooling Potential," 23rd International Space Technology and Science Conf., Paper ISTS 2002-a-29, Matsue, Japan, May 2002.

[14]Liang, K., Yang, B., and Zhang, Z., "Investigation of Heat Transfer and Coking Characteristics of Hydrocarbon Fuels," *Journal of Propulsion and Power*, Vol. 14, No. 5, 1998, pp. 789–796.

[15]Hald, H., Ortelt, M., Fischer, I., Greuel, D., "CMC Rocket Combustion Chamber with Effusion Cooling," 54th International Astronautical Congress, Paper IAC-03-S.P.22, Sept. 2003.

T. Lin
Associate Editor